Applied Catalysis B: Environmental 89 (2009) 309–314

Contents lists available at ScienceDirect

Applied Catalysis B: Environmental

journal homepage: www.elsevier.com/locate/apcatb

A novel synthesis of carbon-coated anatase nanocrystals showing high adsorption capacity and photocatalytic activity

Yu-Chuan Hsu, Huang-Ching Lin, Chien-Wei Lue, Yi-Ting Liao, Chia-Min Yang *

Department of Chemistry, National Tsing Hua University, Hsinchu 30013, Taiwan

ARTICLE INFO

Article history:
Received 22 September 2008
Received in revised form 2 December 2008
Accepted 6 December 2008
Available online 24 December 2008

Keywords:
Anatase nanocrystals
Carbon coating
Dye adsorption
Methylene blue photodecomposition

ABSTRACT

Anatase nanocrystals coated with thin and uniform carbon layer have been prepared directly by using molecular precursors of titanium tetrachloride as a titanium source and fructose as a carbon source in benzyl alcohol. The anatase nanoparticles thus prepared possess high crystallinity, and the carbonaceous species from the dehydrated sugar coat the nanoparticles and transform to uniform and thin carbon layer with graphitic nature. The thus prepared carbon-coated anatase nanocrystals exhibit fast adsorption of methylene blue with high capacity, and they also catalyze the photodecomposition of the dye with greatly enhanced activity. The synthesis route provides rational control over the properties of carbon-coated anatase nanocatalysts for practical applications.

1. Introduction

Photocatalytic degradation is an attractive method to remove organic pollutants in water and in air [1], and anatase titanium dioxide (TiO_2) with high photocatalytic activity, excellent stability and low cost is regarded as the most promising photocatalyst [2–8]. The crystallinity of anatase TiO_2 can be improved by high temperature treatment which is, however, often concomitant with sintering and transformation to rutile or other phases with poor photoactivity. A way to retard these processes is to coat the TiO_2 with carbon layer [9–15], which further renders higher adsorptivity for organic pollutants due to its microporous nature [13,16]. However, the reported coating processes have limited control over the uniformity and the thickness of the carbon layer, and significant reduction of ultraviolet (UV) radiation reaching TiO_2 may occur if the layer is not uniform and thin enough [13,14].

We herein report a simple, direct and high-yield synthesis of carbon-coated nanocrystalline anatase in a mixture of benzyl alcohol, titanium tetrachloride ($TiCl_4$) and fructose. The reaction system of benzyl alcohol and metal chlorides is a versatile nonaqueous process to anatase and other metal oxide nanoparticles [17–23]. Interestingly, we discovered that the formation of the nanocrystalline anatase is not disturbed by the presence of fructose, a monosaccharide with multiple hydroxyl groups. In addition, the carbonaceous species produced by the dehydration of the sugar can be directly deposited on to the TiO_2 nanocrystals, which can be further pyrolyzed to form a thin and uniform carbon layer with graphitic nature. As compared with other carbon-coated TiO_2 nanoparticles [9,11,13–15], the thus prepared photocatalysts with optimized structural properties exhibit high adsorption capacity for methylene blue (MB) and greatly enhanced activity for the photocatalytic decomposition, and the disclosed preparation can be easily up-scaled for mass production for practical applications.

2. Experimental

2.1. Synthesis

D-Fructose was first dispersed in benzyl alcohol in an inert nitrogen atmosphere, and $TiCl_4$ was then slowly added under vigorous stirring at room temperature for 1 h. The molar composition was $1TiCl_4$:0.42D-fructose:20 benzyl alcohol. The synthesis mixture was then sealed in a reaction vessel and was stirred at 80 °C for 24 h. The resulting suspension, dark brown in color, was centrifuged at 6000 rpm for 20 min. The precipitate was then re-dispersed and washed with chloroform and was again centrifuged to remove the solvent, and this procedure was further repeated twice with ethanol. Finally, the material was dried in vacuum at room temperature and was ground into fine powder (designated as TF-syn). For comparison, a material (designated as T-syn) was prepared without the addition of D-fructose in the

* Corresponding author at: Department of Chemistry, National Tsing Hua University, No. 101, Sec. 2, Kuang-Fu Rd., Hsinchu 30013, Taiwan.
Tel.: +886 3 5731282; fax: +886 3 5165521.
E-mail address: cmyang@mx.nthu.edu.tw (C.-M. Yang).

0926-3373/$ – see front matter © 2008 Elsevier B.V. All rights reserved.
doi:10.1016/j.apcatb.2008.12.008

synthesis mixture. The samples TF-syn and T-syn were heated at 300–900 °C in vacuum for 2 h with a ramping rate of 1 °C min^{-1} to pyrolyze the carbonaceous species. The pyrolyzed samples are designated as TF-*x* or T-*x*, where *x* denotes the pyrolysis temperature.

2.2. Characterizations

Thermogravimetric analysis was performed using a Seiko SSC 5000-TG/DTA thermal analyzer in air flow of 100 mL min^{-1} with a heating rate 10 °C min^{-1} from room temperature to 1000 °C. The content of carbonaceous species was estimated from the weight loss between 200 and 600 °C. PXRD data were obtained on a Mac Science 18MPX diffractometer using Cu Kα radiation. Nitrogen physisorption isotherms were measured at 77 K using a Quantachrome Autosorb-1MP instrument. All the samples were evacuated at 80 °C for 12 h before measurements. The BET surface area was calculated from the adsorption branch in the relative pressure range of 0.05–0.30, and the total pore volume was evaluated at a relative pressure of 0.995. The micropore surface area and the micropore volume were estimated by applying the NLDFT method with the model of nitrogen adsorbed on carbon (for TF-*x* samples) or on oxide surface (for TF-syn, Degussa P25 and ISK (Ishihara Sangyo Kaisha) ST-21). The TEM images were obtained with a JEOL JEM-2010 electron microscope operating at 200 kV. XPS spectra were collected on a Physical Electronics PHI 1600 spectrometer with a Mg Kα X-ray source. Raman spectrum was taken on a Triax 550 Jobin Yvon spectrometer using a He–Ne laser with an excitation wavelength of 632.8 nm. The UV–visible absorption spectra of the samples were recorded on a JASCO V-650 spectrophotometer equipped with a diffuse reflection accessory.

2.3. Adsorption and photocatalytic decomposition of MB

A MB solution with a concentration of 1.22×10^{-5} M was prepared by dissolving the dye in purified water, and the solution pH was about 6.5. A TiO_2 sample (25 mg) was then dispersed into the MB solution (200 mL) under ultrasonication. The mixture was stirred in the dark, and the fading of the blue color of the dye was monitored by measuring the optical absorbance at a wavelength of 665 nm on a JASCO V-650 UV-visible spectrophotometer, from which the concentrations of MB in solutions were calculated from a calibration curve. Prior to the optical measurement, the TiO_2 sample was removed by centrifugation at 9000 rpm for 20 min.

For the study of the photocatalytic decomposition of MB, the same suspension of TiO_2 sample in the MB solution was prepared in a quartz reactor. After stirring in the dark for 6 h to reach the adsorption equilibrium, the mixture was exposed to the UV irradiation from an Oriel 150 W xenon lamp together with a UV band-pass filter (UG11, bandwidth of 200–400 nm). The power density of the UV irradiation on the mixture was measured 1.7 mW cm^{-2}. The decomposition proceeded under aerobic (oxygen-saturated) conditions and the mixture was magnetically stirred throughout the irradiation. The decomposition of MB was followed by measuring the optical absorbance of the solution at 660 nm as a function of irradiation time, and the solid sample was removed by centrifugation prior to the measurement.

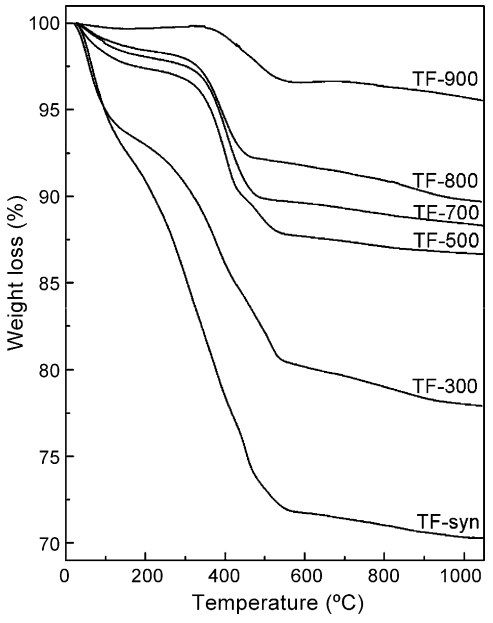

Fig. 1. TGA data of TF-syn and the samples after pyrolysis at various temperature.

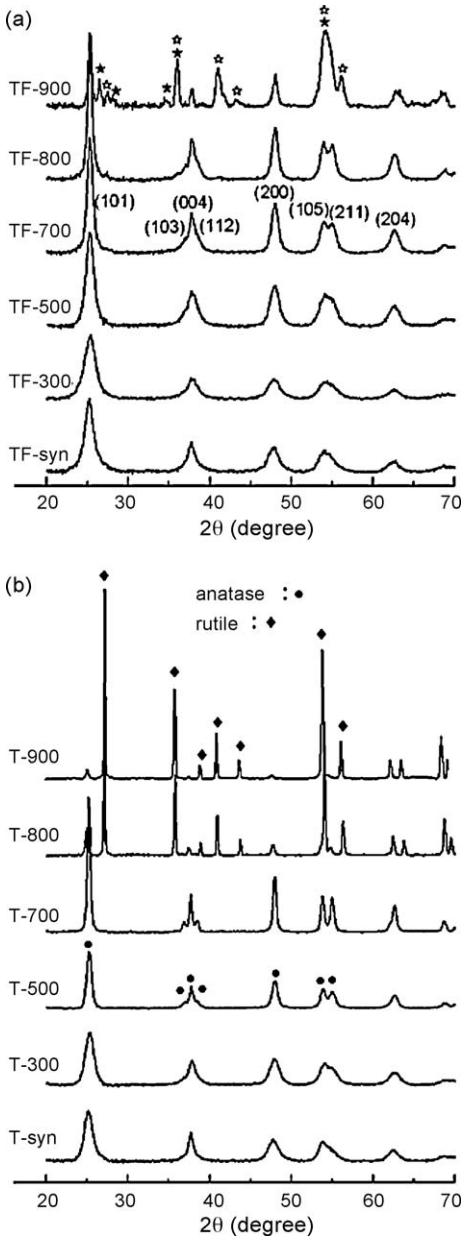

Fig. 2. (a) PXRD patterns of TF-syn and the samples after pyrolysis at various temperature. Reflections from rutile (☆) and reduced phase (★) are indicated. (b) PXRD patterns of T-syn and the samples after pyrolysis at various temperature.

3. Results and discussion

3.1. Carbon-coated TiO_2 nanoparticles

The as-synthesized sample TF-syn is a dark brown powder in excellent yield (>90%) based on the titanium content. The thermogravimetric analysis (TGA) curve (Fig. 1) shows that it contains about 21.1 wt% of carbonaceous species. The dehydration of fructose may be catalyzed by hydrogen chloride generated from $TiCl_4$ by reacting with benzyl alcohol and residual water in the synthesis mixture, and probably also catalyzed by $TiCl_4$ itself. TF-syn gives a powder X-ray diffraction (PXRD) pattern in Fig. 2a with broad reflections attributed to small anatase nanocrystals without the presence of other phases. The crystallite size is estimated 6.2 nm from the width of the (1 0 1) reflection using the Scherrer equation and is very close to the value for the sample (T-syn) prepared from a fructose-free synthesis mixture (Fig. 2b) [22]. The nanocrystalline nature of TF-syn is further confirmed by its transmission electron microscopy (TEM) image and the electron diffraction pattern shown in Fig. 3a. The results clearly show that the presence of fructose in the synthesis mixture had little influence on the formation of the Ti–O–Ti bonds of anatase phase [21,24] despite the possible interfering reactions between $TiCl_4$ and the hydroxyl groups of fructose and the water generated by its dehydration.

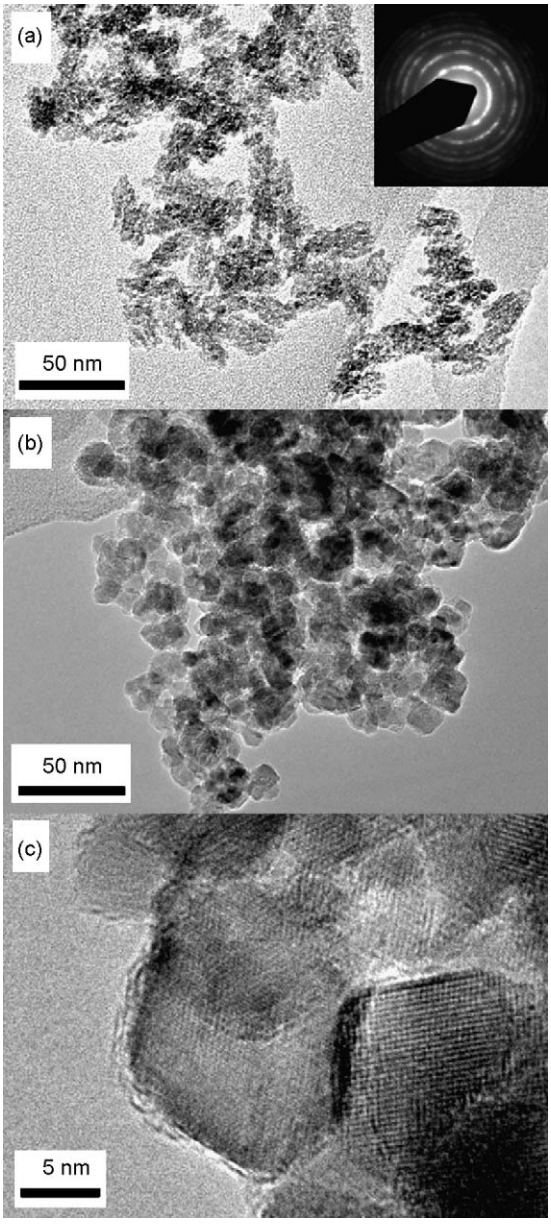

Fig. 3. TEM images of TF-syn (a) and TF-800 (b and c).

Table 1
Characteristics of the TiO_2 photocatalysts studied in the present work[a].

Samples	W_c/wt%	D_a/nm	S_{BET}/$m^2\,g^{-1}$	V_t/$cm^3\,g^{-1}$	C_{MB}/%	k_{app}/$10^{-3}\,min^{-1}$
TF-syn	21.1	6.2	256	0.57	0.7	0.6
TF-300	13.8	4.9	272	0.55	1.1	0.6
TF-500	10.0	8.2	185	0.57	66.1	5.2
TF-700	8.6	13.3	153	0.49	74.2	6.4
TF-800	6.8	14.5	135	0.44	73.7	7.7
TF-900	3.1	16.7	109	0.43	42.6	1.6
P25	0	20 (25)[b]	51	0.72	NA[c]	1.4
ST-21	0	20	61	0.84	NA[c]	1.7

[a] W_c: content of carbonaceous species; D_a: crystallite size of the anatase phase; S_{BET}: BET surface area; V_t: total pore volume; C_{MB}: amount of MB adsorbed from a 1.22×10^{-5} M MB solution; k_{app}: apparent first-order rate constant for MB photodecomposition.
[b] Crystallite size of the rutile phase in the sample.
[c] Not available.

The sample TF-syn was heated at 300–900 °C in vacuum for 2 h to pyrolyze the carbonaceous species. TGA data (Fig. 1) indicate that the carbonaceous content decreases from 13.8 wt% for TF-300 to 6.8 wt% and 3.1 wt% for TF-800 and TF-900, respectively. All the samples except TF-900 give PXRD patterns exclusively from the anatase phase (Fig. 2a), and the crystallite size slightly increases with increasing the heating temperature (Table 1). Since the anatase-to-rutile transformation was already observed between 700 and 800 °C for the materials synthesized from a fructose-free solution (cf. Fig. 2b), the results suggest that the pyrolyzed carbonaceous species suppressed the structural transformation at high temperature. The heat treatment also improves the crystallinity of the anatase phase, and the broad and overlapped reflections for TF-300 (i.e. the (1 0 3), (0 0 4) and (1 1 2) reflections and the (1 0 5) and (2 1 1) reflections) become resolved for TF-700 and TF-800. At 900 °C, most of the anatase nanocrystals were either transformed to rutile phase or reduced to Ti_4O_7 by the coated carbon species [9,14,15].

The carbon-coated samples were further characterized by nitrogen physisorption measurement. As shown in Fig. 4, each sample gives an isotherm exhibiting a sharp step with a H1-type hysteresis loop corresponding to a uniform textural mesoporosity in the sample composed of uniform nanoparticles. The sample treated at higher temperature has larger nanoparticles and therefore larger textual mesopores (cf. Table 1). Furthermore, the surface areas for the samples heated at 500–900 °C are not so large as expected for those coated with similar amount of porous carbon [9,13,16] but are very close to the values estimated from the anatase size by assuming a model structure composed of hard spheres [22,25]. The NLDFT analysis also reveals very small micropore surface areas (7–20 $m^2\,g^{-1}$) and micropore volumes (below 0.01 $cm^3\,g^{-1}$) for these samples. In line with this finding, the TEM images of TF-800 (Fig. 3b and c) shows that most of the carbon-coated anatase nanocrystals with sizes of 12–17 nm form aggregates with retained textural porosity, and separate particles are seldom found. In addition, each anatase nanocrystal is uniformly coated with thin carbon (0.8–1.5 nm in thickness) composed of graphene layers. The graphitic nature of the thin carbon layer in TF-800 was further confirmed by the sharp peak at 284.4 eV in the XPS spectrum of the C 1s region in Fig. 5a [26] and the narrow G band in the Raman spectrum in Fig. 5b. It is also interesting to find that separate particles are seldom observed and most of the carbon-

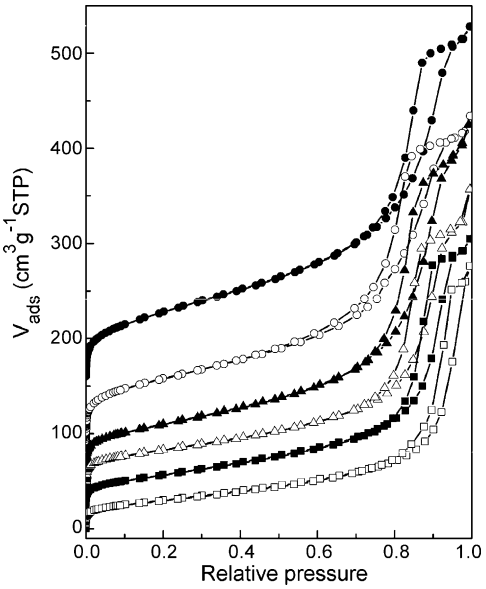

Fig. 4. Nitrogen physisorption isotherms of TF-syn (●), TF-300 (○), TF-500 (▲), TF-700 (△), TF-800 (■) and TF-900 (□) shifted by 160, 80, 60, 40, 20 and 0 $cm^3 g^{-1}$ STP, respectively.

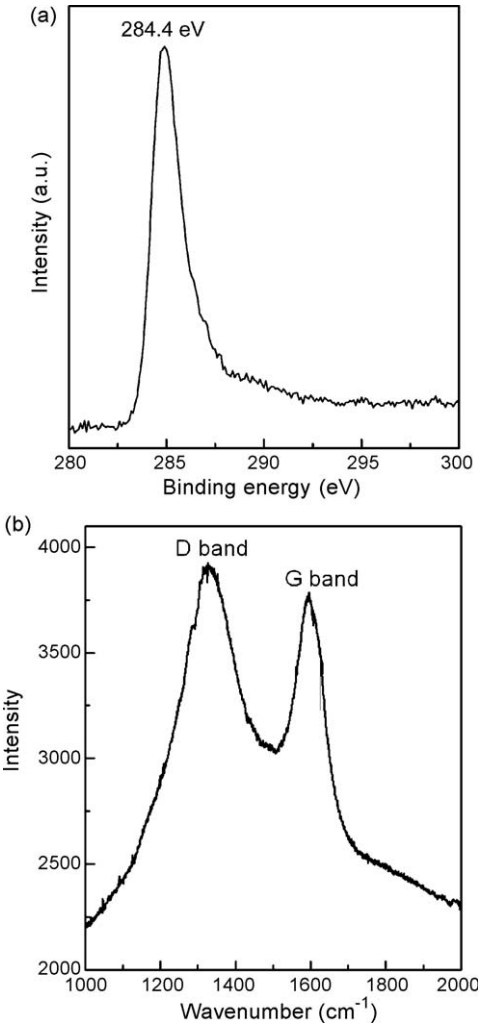

Fig. 5. XPS spectrum of the C 1s region (a) and Raman spectrum (b) for TF-800.

coated anatase nanocrystals are glued together, possibly by the residual carbon, to form aggregates (Fig. 3b).

3.2. Adsorption of MB on carbon-coated TiO_2 nanoparticles

Methylene blue is a brightly colored blue cationic thiazine dye and is often used as a test model pollutant in semiconductor photocatalysis [9,11,13–15]. The dye was chosen in this study in order to compare the adsorption capacity and the photoactivity of the thus prepared carbon-coated anatase nanocrystals with those of the reported TiO_2 materials. MB readily forms dimers in aqueous solution, and a typical value for the equilibrium constant associated with the dimerisation process is 3970 L mol^{-1} [27]. Given that the total MB concentration of 1.22×10^{-5} M, about 93% of the dye was estimated to be in its monomer form and the amount of dimer present in solution can be considered negligible.

In Fig. 6 the change of the relative concentration of MB in solution in the dark is shown. While TF-syn and TF-300 only adsorb very small amount of MB, other samples exhibit marked and fast adsorption of MB. About 74% of the dye molecules were adsorbed within 30 min for TF-700 and TF-800 with thin carbon coating. It is believed that the main driving forces for the dye adsorption are the hydrophobic interactions and π–π interactions between the graphitic carbon layer and the aromatic rings of the dye molecules. The adsorption studies of TF-800 with other organic compounds (including Rhodamine 6G, eosin dyes and 4-nitrophenol) were also performed, and similar results of fast adsorption and high adsorption capacity were observed. In addition, the photograph in Fig. 6 shows that the samples can be easily separated from the solution by sedimentation, probably due to the aggregation of carbon-coated nanocrystals as revealed previously by TEM in these samples. In comparison, the commercial TiO_2 materials P25 and ST-21 showed very little MB adsorption and the solid could only be

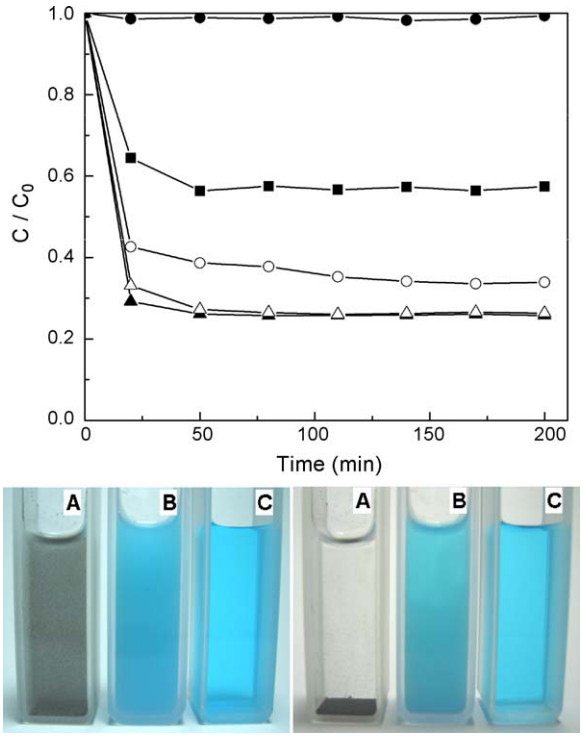

Fig. 6. *Top*: Change in relative concentration of MB in the dark with time due to the adsorption by TF-syn (●), TF-500 (○), TF-700 (▲), TF-800 (△) and TF-900 (■). *Bottom*: Photographs of 20 mg TF-800 (A) or P25 (B) in 20 mL 1.2×10^{-5} M MB solution upon mixing (left) and after 40 min (right). The photographs of a pure MB solution (C) are also shown for comparison.

separated by centrifugation. The simple separation by sedimentation increases the potential of the carbon-coated photocatalysts for water treatment system [1]. For TF-900, its significantly decreased adsorption capacity may be related to a reduced surface area and lowered carbon content of the sample.

3.3. Photodecomposition of MB by carbon-coated TiO_2 nanoparticles

To evaluate the photocatalytic activity of the thus prepared TiO_2 photocatalysts, the TiO_2-sensitized photodecomposition of MB under UV irradiation was investigated. The photobleaching of MB can be due to either the oxidative degradation of the dye [28–30] or a reduction to its leuco form (LMB) by a reducing agent that could be water or MB itself [30–32]. The conditions that favor the formation of LMB include a low oxygen level and a low pH, but LMB can be again oxidized to regenerate MB by oxygen dissolved in solution [30,31]. In this study, the reaction mixtures were at pH 6.5, oxygen-saturated and were continuously stirred throughout UV irradiation. The conditions avoided the reduction of MB and facilitated the oxidation of LMB, if any produced during the reaction. Therefore, the observed photobleaching should be mainly attributed to the oxidative photodegradation of the dye sensitized by TiO_2. An alternative way to follow the degradation of MB is to measure the evolution of carbon dioxide generated by the reaction [28]. However, CO_2 evolution has been shown to occur at a much slower rate than MB bleaching because many different intermediates are involved in oxidative mineralization of MB [28,30]. Therefore, the measurement of dye bleaching instead of CO_2 evolution was chosen for this study.

Before studying and comparing the activities of various TiO_2 materials, the bleaching of MB in the absence of any catalysts was first examined. This is because the dye also absorbs the UV light between 200 and 400 nm (Fig. S1 in the Supplementary Information) and the photoexcited dye may be reduced to LMB or be oxidized and decomposed. Fig. 7a shows the curves of the change in relative concentration of MB (calculated from the absorption at 665 nm) absorption versus irradiation time with or without the presence of TiO_2 catalysts. It was found that about 9% of the dye was bleached, in the absence of any photocatalysts, after an irradiation time of 360 min. The irradiated solution was subsequently purged with oxygen for hours, and the blue color of the solution did not get more intense. It suggests that there was very limited amount of LMB produced by photoreduction of MB [30], and that the observed bleaching would be mainly attributed to oxidative degradation of the photoexcited dye under the irradiation conditions of low power density of 1.7 mW cm^{-2}.

Next, the photoactivity of the commercial and thus prepared TiO_2 materials was studied. In order to follow the color fading purely due to the catalytic decomposition, all the catalysts were saturated with MB prior to any irradiation. In addition, the amounts of the self-degradation of the photoexcited dye were also subtracted from the observed values in the experiments. For the commercial TiO_2 materials P25 and ST-21, about 47–53% of MB was decomposed after irradiating UV light for 360 min. The activity of ST-21 was a bit better than that of P25, probably due to its pure anatase phase in comparison to the mixed anatase–rutile phases of P25. For TF-500, TF-700 and TF-800, surprisingly, around 87–97% of the dye was degraded after the same duration of UV irradiation. Again, nearly no LMB was found in the irradiated solutions (Fig. S1 in the Supplementary Information). The superior photoactivity of these carbon-coated materials also implied that the thin carbon layer on the anatase nanocrystals might still allow the charge carriers generated upon UV absorption to migrate to the surface to initiate the decomposition of the adsorbed dye molecules. For TF-900 with mixed crystalline phases, it exhibited a low but comparable photoactivity to the commercial catalysts. For the carbon-coated

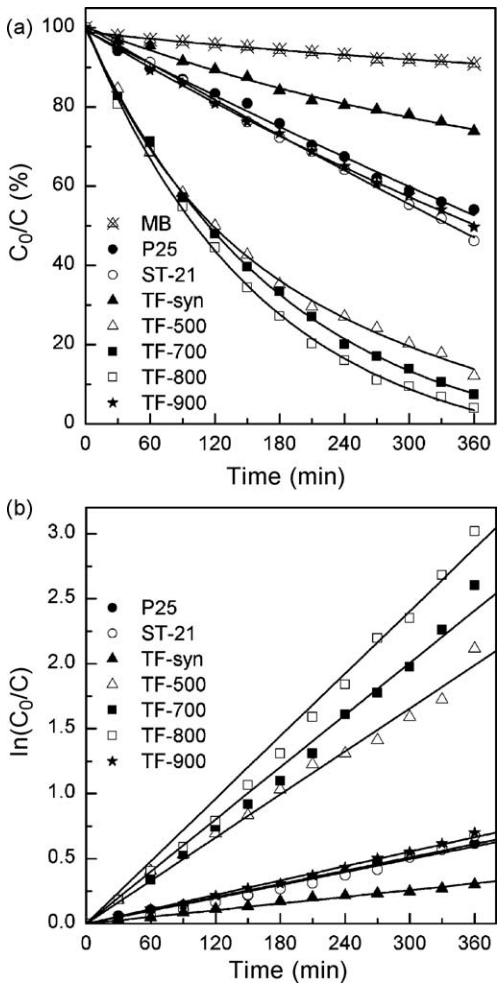

Fig. 7. (a) Change in relative concentration of MB with UV irradiation time in the absence or presence of TiO_2 photocatalysts. (b) Transformed linear graph of $\ln(C_0/C)$ versus irradiation time.

samples, unfortunately, the light intensity reaching TiO_2 nanocrystals could not be precisely controlled to have a fair comparison of reaction rates and activities because of the absorption and scattering of light by the coating layer of carbonaceous species or graphitic carbon [33]. The UV–visible spectra of these samples and the carbon-free sample prepared by further calcining TF-800 at 500 °C in air (Figs. S2 and S3 in the Supplementary Information) indicate that in addition to the high absorption for the visible light, the carbon coatings also showed different degree of low absorption in the UV region, depending on the amount and chemical nature of the coated carbon. The results suggest that the intensity of UV irradiation on the TiO_2 nanocrystals in the carbon-coated materials was indeed lower than that on the commercial P25 and ST-21 materials under the same irradiation conditions, which in turn implied that the photoactivity of the coated anatase nanocrystals might be possibly underestimated.

The data in Fig. 6a were further transformed into the logarithm plots in Fig. 7b. The relations between $\ln(C/C_0)$ and time for various TiO_2 materials were found approximately linear, suggesting that the overall kinetics of the photodecomposition reactions were first-order with respect to the dye concentration. The apparent rate constants calculated from the slopes of linear relations were listed in Table 1. For samples TF-500, TF-700 and TF-800, the rate constants were much higher than those for the commercial TiO_2 materials, and TF-800 even showed a rate constant 5.5 times higher than that for P25. Such an enhancement in the activity for

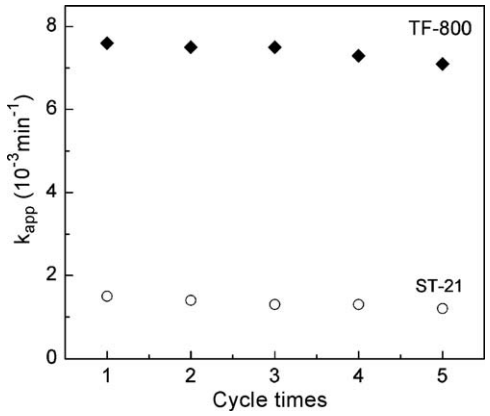

Fig. 8. Changes in apparent rate constant with cycling operations of photodecomposition on TF-800 or ST-21.

the photodecomposition of MB is larger than other reported carbon-coated TiO_2 materials [9,11,13–15]. The high activity observed for TF-800 may be partly attributed to its highly crystalline anatase phase [2–4,34]. On the other hand, although the thin carbon coating inevitably weakened the UV irradiation on the anatase nanocrystals, it largely enhanced the dye adsorption and could also facilitate the overall decomposition kinetics by increasing the local concentration of MB. Since the adsorbed dye molecules were in the vicinity of the anatase nanocrystals, their photoexcitation might also lead to an oxidation by direct electron transfer to TiO_2 [2–4,30]. The graphitic carbon layer itself may also play a role as a photosensitizer, generate electron–hole pairs and transfer electrons to the conduction band of metal oxides [35,36]. However, the holes thus generated might not have sufficient oxidation power to degrade the dye molecules. It has to be mentioned that the carbon-coated anatase phase might be doped with carbon during the pyrolysis at high temperature [37], and contribution of possible carbon doping to the photocatalytic activity could not be excluded. The clues for the possible carbon doping are from the slight shift of UV–visible absorption bands of the carbon-coated samples (cf. Fig. S2) and the calculated band gaps (3.16 eV for TF-syn and 3.14 eV for TF-800) from the plots of the modified Kubelka–Munk function versus the energy of exciting light, assuming that the materials are indirect semiconductors. In addition, XPS spectrum of the Ti 2p region for TF-800 also show slight shift as compared to the spectrum of T-syn (Fig. S4 in the Supplementary Information).

Finally, TF-800 and ST-21 were selected to test cyclic performances of MB decomposition. The photocatalysts were separated from the solution after the reaction by sedimentation (for TF-800) or by centrifugation (for ST-21), and were used for the adsorption and degradation of fresh samples of MB following the same procedures and irradiation conditions. Fig. 8 shows the calculated apparent rate constants for the two catalysts with cycling operations. TF-800 exhibited rather good and stable activity, and the rate constants just slightly decreased (about 6%) from 7.6×10^{-3} min^{-1} for the first cycle to 7.1×10^{-3} min^{-1} for the fifth cycle. In comparison, the rate constant for ST-21 showed a decrease of 13% after being reused for five times. The results suggest that cyclic usage of the highly efficient TF-800 photocatalyst is possible and its stability in treating polluted water is satisfactory.

4. Conclusions

We have developed a direct and high-yield synthesis of highly crystalline anatase nanoparticles coated with thin and uniform carbon layer with graphitic nature. The thus prepared photocatalysts show fast adsorption of methylene blue with high capacity, and they also catalyze the photodecomposition of the dye with greatly enhanced activity. The disclosed synthesis provides rational control over the properties of carbon-coated anatase nanocatalysts for practical applications.

Acknowledgements

We thank the National Science Council, Taiwan for financial support under the contract nos. NSC 95-2113-M-007-032-MY3 and NSC 96-2120-M-002-007.

Appendix A. Supplementary data

Supplementary data associated with this article can be found, in the online version, at doi:10.1016/j.apcatb.2008.12.008.

References

[1] T. Wakanabe, A. Kitamura, E. Kojima, C. Nakayama, K. Hashimoto, A. Fujishima, Photocatalytic Purification and Treatment of Water and Air, Elsevier, Amsterdam, 1993.
[2] M.R. Hoffmann, S.T. Martin, W. Choi, D.W. Bahnemann, Chem. Rev. 95 (1995) 69–96.
[3] A.L. Linsebigler, G. Lu, J.T. Yates, Chem. Rev. 95 (1995) 735–758.
[4] X. Chen, S.S. Mao, Chem. Rev. 107 (2007) 2891–2959.
[5] G.J.A.A. Soler-Illia, J. Patarin, B. Lebeau, C. Sanchez, Chem. Rev. 102 (2002) 4093–4138.
[6] F. Schüth, Angew. Chem. Int. Ed. 42 (2003) 3604–3622.
[7] M.H. Bartl, S.W. Boettcher, K.L. Frindell, G.D. Stucky, Acc. Chem. Res. 38 (2005) 263–271.
[8] C. Aprile, A. Croma, H. Carcia, Phys. Chem. Chem. Phys. 10 (2008) 769–783.
[9] T. Tsumura, N. Kojitani, I. Izumi, N. Iwashita, M. Toyoda, M. Inagaki, J. Mater. Chem. 12 (2002) 1391–1396.
[10] M. Janus, M. Tryba, M. Inagaki, A.W. Morawski, Appl. Catal. B: Environ. 52 (2004) 61–67.
[11] L. Lin, W. Lin, Y.X. Zhu, B.Y. Zhao, Y.C. Xie, Y. He, Y.F. Zhu, J. Mol. Catal. A: Chem. 236 (2005) 46–53.
[12] M. Janus, M. Inagaki, B. Tryba, M. Toyoda, A.W. Morawski, Appl. Catal. B: Environ. 63 (2006) 272–276.
[13] M. Inagaki, F. Kojin, B. Tryba, M. Toyoda, Carbon 43 (2005) 1652–1659.
[14] B. Tryba, A.W. Morawski, T. Tsumura, M. Toyoda, M. Inagaki, J. Photochem. Photobiol. A: Chem. 167 (2004) 127–135.
[15] T. Matsunaga, M. Inagaki, Appl. Catal. B: Environ. 64 (2006) 9–12.
[16] M. Inagaki, S. Kobayashi, F. Kojin, N. Tanaka, T. Morishita, B. Tryba, Carbon 42 (2004) 3153–3158.
[17] R.J.P. Corriu, D. Leclercq, Angew. Chem. Int. Ed. 35 (1996) 1420–1436.
[18] A. Vioux, Chem. Mater. 9 (1997) 2292–2299.
[19] J.N. Hay, H.M. Raval, J. Sol–Gel Sci. Technol. 13 (1998) 109–112.
[20] M. Inoue, J. Phys. Condens. Matter. 16 (2004) S1291–S1303.
[21] M. Niederberger, G. Garnweitner, Chem. Eur. J. 12 (2006) 7282–7302.
[22] M. Niederberger, M.H. Bartl, G.D. Stucky, Chem. Mater. 14 (2002) 4364–4370.
[23] M. Niederberger, M.H. Bartl, G.D. Stucky, J. Am. Chem. Soc. 124 (2002) 13642–13643.
[24] G. Garnweitner, M. Niederberger, J. Mater. Chem. 18 (2008) 1171–1182.
[25] M.S. Wong, E.S. Jeng, J.Y. Ying, Nano Lett. 1 (2001) 637–642.
[26] C.M. Yang, C. Weidenthaler, B. Spliethoff, M. Mayanna, F. Schüth, Chem. Mater. 17 (2005) 355–358.
[27] W. Spencer, J.R. Sutter, J. Phys. Chem. 83 (1979) 1573–1576.
[28] R.W. Matthews, J. Chem. Soc., Faraday Trans. 1 (85) (1989) 1291–1302.
[29] S. Lakshmi, R. Renganathan, S. Fujita, J. Photochem. Photobiol. A: Chem. 88 (1995) 163–167.
[30] A. Mills, J. Wang, J. Photochem. Photobiol. A: Chem. 127 (1999) 123–134.
[31] H. Yoneyama, Y. Toyoguchi, H. Tamura, J. Phys. Chem. 76 (1972) 3460–3463.
[32] N.R. de Tacconi, J. Carmona, K. Rajeshwar, J. Electrochem. Soc. 144 (1997) 2486–2490.
[33] M. Chhowalla, H. Wang, N. Sano, K.B.K. Teo, S.B. Lee, G.A.J. Amaratunga, Phys. Rev. Lett. 90 (2003) 155504–155507.
[34] M. Toyoda, Y. Nanbu, Y. Nakazawa, M. Hirano, M. Inagaki, Appl. Catal. B: Environ. 49 (2004) 227–232.
[35] T. Umeyama, N. Tezuka, M. Fujita, S. Hayashi, N. Kadota, Y. Matano, Chem. Eur. J. 14 (2008) 4875–4885.
[36] Y. Ou, J. Lin, S. Fang, D. Liao, Chem. Phys. Lett. 429 (2006) 199–203.
[37] S. Sakthivel, H. Kisch, Angew. Chem. Int. Ed. 42 (2003) 4908–4911.